BIOCHEMISTRY
including biophysical chemistry & molecular biology

Article

pubs.acs.org/biochemistry

Aldolases Utilize Different Oligomeric States To Preserve Their Functional Dynamics

Ataur R. Katebi† and Robert L. Jernigan*

L. H. Baker Center for Bioinformatics and Biological Statistics, Department of Biochemistry, Biophysics and Molecular Biology, and Interdepartmental Program for Bioinformatics and Computational Biology, Iowa State University, Ames, Iowa 50011-3020, United States

Supporting Information

ABSTRACT: Aldolases are essential enzymes in the glycolysis pathway and catalyze the reaction cleaving fructose/tagatose 1,6-bisphosphate into dihydroxyacetone phosphate and glyceraldehyde 3-phosphate. To determine how the aldolase motions relate to its catalytic process, we studied the dynamics of three different class II aldolase structures through simulations. We employed coarse-grained elastic network normal-mode analyses to investigate the dynamics of *Escherichia coli* fructose 1,6-bisphosphate aldolase, *E. coli* tagatose 1,6-bisphosphate aldolase, and *Thermus aquaticus* fructose 1,6-bisphosphate aldolase and compared their motions in different oligomeric states. The first one is a dimer, and the second and third are tetramers. Our analyses suggest that oligomerization not only stabilizes the aldolase structures, showing fewer fluctuations at the subunit interfaces, but also allows the enzyme to achieve the required dynamics for its functional loops. The essential mobility of these loops in the functional oligomeric states can facilitate the enzymatic mechanism, substrate recruitment in the open state, bringing the catalytic residues into their required configuration in the closed bound state, and moving back to the open state to release the catalytic products and repositioning the enzyme for its next catalytic cycle. These findings suggest that the aldolase global motions are conserved among aldolases having different oligomeric states to preserve its catalytic mechanism. The coarse-grained approaches taken permit an unprecedented view of the changes in the structural dynamics and how these relate to the critical structural stabilities essential for catalysis. The results are supported by experimental findings from many previous studies.

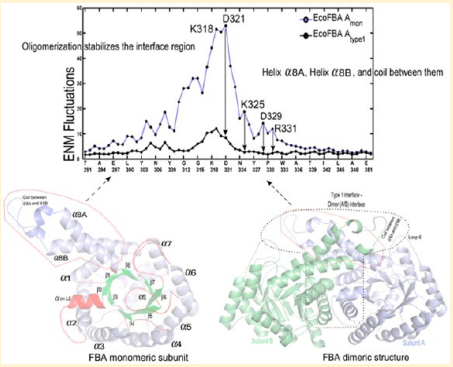

Fructose 1,6-bisphosphate aldolase catalyzes the reversible condensation of two three-carbon sugar substrates, dihydroxyacetone phosphate (DHAP) and glyceraldehyde 3-phosphate (GAP), into a six-carbon fructose 1,6-bisphosphate (FBP). This is a critical step in the pathways of glycolysis, gluconeogenesis, and the Calvin cycle. Aldolases can be effective drug targets because they employ mechanistically distinct cleavage techniques in higher and lower organisms. The class I aldolases found in higher organisms form a covalent Schiff base intermediate between the DHAP moiety of the substrate and an ε-amino group of an active-site lysine residue during catalysis.[1−3] Alternatively, the class II aldolases found in lower organisms, such as bacteria and fungi, employ a divalent cation, usually Zn^{2+}, Fe^{2+}, Co^{2+}, or Cd^{2+}, as an electrophile in the catalytic cycle.[3−8] Despite a low degree of sequence identity among the aldolases, the key residues and the structural architecture in each class are well-conserved.

Here we consider three representative class II aldolases: two fructose 1,6-bisphosphate aldolase (FBA, EC 4.1.2.13) structures (one from mesophilic bacterium *Escherichia coli* and the other from hyperthermophilic bacterium *Thermus aquaticus*) and one tagatose 1,6-bisphosphatase aldolase (TBA, EC 4.1.2.40) structure from *E. coli*. The class II aldolases function as either dimers or tetramers. *E. coli* FBA has a dimeric structure, whereas *E. coli* TBA and *T. aquaticus* FBA form tetrameric structures.[9,10] Two subunits of an aldolase structure bind together at a type 1 interface to form a functionally active dimeric structure. Two type 1 dimers bind together along two type 2 interfaces and form a functionally active tetrameric structure.

Oligomerization through type 1 and type 2 interfaces (panels A and B of Figure 1, respectively) modifies the dynamics of the aldolase structure and is facilitated by two locks, lock 1 and lock 2, to form higher-order structures. Lock 1 at the type 1 interface is formed through the interaction of helices 1 and 2 from subunit A with helices 1 and 2 from subunit B, and vice versa. Lock 2 of the type 1 interface is formed through the interaction of helix 1 from subunit A with helices 8A and 8B from subunit B, and vice versa. Further details of the locking mechanism in the type 1 interface are depicted in Figure S1 of the Supporting Information. On the other hand, lock 1 at the type 2 interface is formed through the interaction of helices 3 and 4 from subunit A with helix 3 of subunit D, and lock 2 through the binding of

Received: January 17, 2015
Revised: April 27, 2015
Published: May 18, 2015

DOI: 10.1021/acs.biochem.5b00042
Biochemistry 2015, 54, 3543−3554

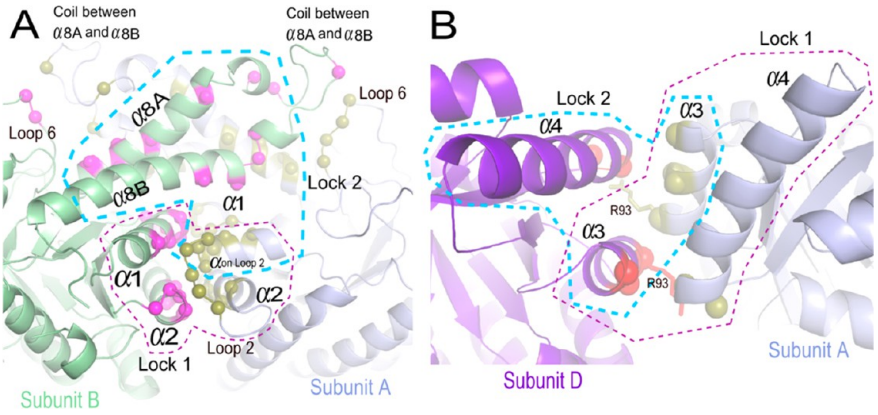

Figure 1. Structural components of type 1 and type 2 interfaces. Panel A shows two locks (lock 1 and lock 2) formed in the type 1 interface in the *E. coli* fructose 1,6-bisphosphate aldolase (FBA) dimeric structure. Panel B shows similar locks (lock 1 and lock 2) formed in a type 2 interface between two subunits in a tetrameric *T. aquaticus* FBA structure. (A) Shown in olive green are the interface-forming residues (C^{α} atoms as spheres) in subunit A (light blue) that are within 5 Å of subunit B (light green). Shown in magenta are the interface-forming residues (C^{α} atoms as spheres) in subunit B that are within 5 Å of subunit A. The secondary structure components of the interface form two locks, lock 1 and lock 2. (B) Lock 1 in the type 2 interface is formed when helices 3 and 4 of subunit A (light blue) form the ridge where helix 3 of subunit D (deep purple) is placed in an antiparallel arrangement, and vice versa for lock 2. The C^{α} atoms on helices 3 and 4 of subunit D within 5 Å of subunit A are shown as red spheres, and the C^{α} atoms on helices 3 and 4 of subunit A within 5 Å of subunit D are shown as olive green spheres.

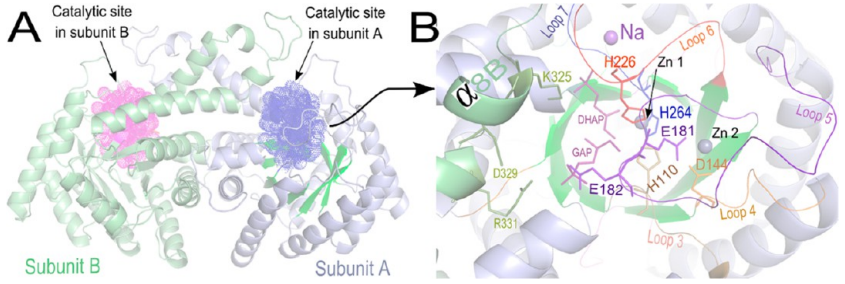

Figure 2. Catalytic environment in an aldolase structure. Panel A shows the catalytic pocket in each subunit of an *E. coli* fructose 1,6-bisphosphate aldolase (FBA) structure (PDB entry 1B57), and panel B shows a close-up of one of the catalytic pockets from panel A. (A) Each subunit has its own catalytic site. Subunit A is colored light blue and subunit B light green. The catalytic sites are marked by mesh structures, blue in subunit A and magenta in subunit B. (B) Close-up of the catalytic pocket in subunit A. K325, D329, and R331 are the three catalytic residues (dark green sticks) from subunit B that play roles in the catalytic environment in subunit A. Dihydroxyacetone phosphate (DHAP) and glyceraldehyde 3-phosphate (GAP), shown as purple sticks, are the products after the cleavage of fructose 1,6-bisphosphate. E181 and E182 (purple sticks) are two catalytically important residues on functional loop 5. Three histidine residues, H110 (gray stick on loop 3), H226 (red stick on loop 6), and H264 (blue stick on loop 7), are the ligands for the first Zn^{2+} ion shown as a gray sphere. One of the ligands for the second Zn^{2+} ion in the open conformation of the structure is D144 (light orange stick) located on loop 4.[11]

helices 3 and 4 of subunit D with helix 3 of subunit A. More about this can be found in Figure S2 of the Supporting Information. We investigate with computations the changes in the dynamics of three aldolase structures in different oligomeric states that are formed through type 1 and type 2 interfaces.

In a functionally active higher-order oligomeric aldolase structure, each subunit has its own catalytic pocket. The spatial positioning of the two catalytic pockets in an *E. coli* FBA dimeric structure is such that the openings of the two pockets are in the opposite direction (blue and magenta pockets in Figure 2A). Figure 2B illustrates the arrangement of the important residues, the substrates, and the relevant secondary structures that form the catalytic microenvironment of such a pocket [Protein Data Bank (PDB) entry 1B57].[11] The residues can be separated into three intersecting groups according to their role in the catalytic environment: (1) substrate and product binding residues, (2) cation binding residues, and (3) catalytic residues. Table S1 of the Supporting Information shows how the residues are distributed into these three functional groups and where, on the structure, they are located in the three aldolases, *E. coli* FBA, *E. coli* TBA, and *T. aquaticus* FBA.[10−12]

Substrate and product binding residues are mainly located on loops 2, 3, 5, and 8 of the host subunit and helices 8A and 8B from the partner subunit. These residues are involved in holding the substrate in the proper catalytic position and binding the products in a suitable way to facilitate their ejection from the catalytic pocket. For example, R331, located on helix 8B in *E. coli* FBA, is involved in binding with substrate.[13] Hall et al. show that A48 in *E. coli* TBA is the equivalent of Q59 in *E. coli* FBA, and the smaller size of alanine compared to that of glutamine helps TBA to accommodate tagatose 1,6-bisphosphate, an alternative conformation of FBP.[10]

Cation binding residues are mainly in loops 3, 4, 6, and 7, and they hold the two divalent Zn^{2+} ions (Zn1, buried at the catalytic pocket; Zn2, at the front of the β-barrel) and one monovalent Na^{+} ion in the catalytically competent positions. When the aldolase structure undergoes the transition from the open to the closed state, the two divalent ions reorient their positions with respect to the monovalent ion, one divalent ion

DOI: 10.1021/acs.biochem.5b00042
Biochemistry 2015, 54, 3543−3554

moving closer to and the other moving away from the monovalent ion (Figure 2B shows an arrangement of these metal ions in a closed *E. coli* FBA structure). The motions of loops 3, 4, 6, and 7 facilitate the divalent ion motions and assist in the proper positioning of the ligand residues to hold the ions in both the open and closed conformations. In the closed conformation, Zn1 is balanced by the scaffold formed by the three histidine residues (H110, H226, and H264 located on loops 3, 6, and 7, respectively) together with the substrate, and Zn2 is balanced by residues D144, E174, and E181 (located on loop 4, strand 5, and loop 5, respectively) and a solvent molecule (H_2O).[9] On the other hand, in the unbound conformation, Zn1 is balanced by residues D109, E172, H264, and K284 (located on loop 3, strand 5, loop 7, and strand 8, respectively), and Zn2 is held by residues H110, E174, H226, and H264 (located on loop 3, strand 5, loop 6, and loop 7, respectively).[14] Mutation of E174, located on the C-terminal end of strand 5 and at the base of loop 5, severely attenuates the catalytic activity of *E. coli* aldolase.[15] This suggests that appropriate flexibility of loop 5 is needed to bring this residue into a suitable position to hold the divalent ion in the open conformation, as well. The Na^+ binding site is 5.6 Å from the Zn1 binding site and is sandwiched between loops 6 and 7. These two cations facilitate the correct active-site alignment of the residues located on these two loops suitable for catalytic function.[9] Hyperthermophilic *T. aquaticus* aldolase is a Co^{2+}-based enzyme, and the monovalent cation is either NH_4^+ (ammonium) or Y^+ (yttrium).[10,12]

Functional loops 3, 5, 7, and 8 include the catalytic residues in each of the structures. Their dynamics are essential for the proper functioning of the catalytic residues.[16] In particular, the critical flexibility of loop 5 in *E. coli* FBA is necessary to place catalytically important residues E181 and E182 on the loop in the proximity of the substrate. A quadruple mutation (G176A/G179A/G180A/G184A) on this loop significantly reduces the enzymatic activity.[15] Loop 5 flexibility allows it to go through a large conformational transition. In the open state, it facilitates substrate recruitment, whereas in the closed state, it places E181 and E182 in their catalytically competent positions. Moreover, mutation of D109, on loop 3, decreases the k_{cat} of the reaction by 300-fold, whereas mutation of N286 located at the N-terminal base of loop 8 causes an 800-fold decrease in the k_{cat} value.[17] D109 and N286 function in a coupled manner for substrate recruitment and product formation: D109 aids the binding of DHAP in the catalytic pocket, whereas N286 facilitates the creation of a new carbon−carbon bond with the incoming GAP, which helps the condensation of the catalytic product FBP. It has further been shown that conformational coupling and dynamics play a role in substrate specificity.[18] K325, located on the coil segment between helices α8A and α8B, is shown to be involved in catalysis and may also support other important residues in forming the catalytic microenvironment in *E. coli*.[11] Thus, the conformational dynamics of the coil brings the catalytic residues on this segment into a catalytically suitable orientation. Further, in the case of functionally tetrameric aldolases, *E. coli* TBA and *T. aquaticus* FBA, the tetrameric form is energetically more favorable than other oligomeric forms. Energy calculations also suggested that tetramer is a dimer of two dimers.[19]

The dynamics of the structural components of the microenvironment and the interface regions are essential for aldolase function. However, there has been a lack of studies showing how the dynamics of these loops are related to the global motions of the aldolase structure. In this research, we employ the elastic network model (ENM)[20] to study the global motions of three aldolase structures: *E. coli* FBA, *E. coli* TBA, and *T. aquaticus* FBA. We investigate how oligomerization influences the stability of each interface. We further investigate how oligomerization affects the dynamics of the functional loops in the catalytic microenvironment. These computations show that oligomerization not only provides needed stability to the aldolases but also allows the structures to achieve the requisite functional dynamics at the catalytic pocket and functional loops.

MATERIALS AND METHODS

Aldolase Structures for Modeling Dynamics. We selected three PDB structures to investigate the dynamics of class II aldolases. Two are class II FBA (EC 4.1.2.13) structures, *E. coli* FBA (EcoFBA) (PDB entry 1B57) and *T. aquaticus* FBA (TaqFBA) (PDB entry 1RVG), and one is a class II TBA (EC 4.1.2.40) structure, *E. coli* TBA (EcoTBA) (PDB entry 1GVF). The biologically active oligomeric state of *E. coli* FBA was found to be a dimer by a gel electrophoresis experiment.[21] On the other hand, *T. aquaticus* FBA was found to be a tetramer in solution studies, indicating it has a tetrameric functional state[12] and the functional oligomeric state of *E. coli* TBA was found to be a tetramer as determined by gel filtration studies.[11,22] For *E. coli* FBA (PDB entry 1B57), the asymmetric unit and the biological unit appear to be the same. For the latter two structures, we retrieved their tetrameric states from PDB entries 1RVG and 1GVF, respectively, using the crystallographic symmetry information available within the respective coordinate file. We find support for the tetrameric structures in our findings where the particular details in the tetramer are necessary to make its dynamics more similar to the dynamics observed for the dimeric structures.

We computed sequence conservation scores of the aldolases using the ConSurf server.[23] The structural components around the catalytic pocket are found to be highly conserved (details in Figure S4 of the Supporting Information). We also computed the areas of subunits and interfaces using the PISA server.[24] Tetrameric *E. coli* TBA and *T. aquaticus* FBA structures are found to have more compact subunits than the dimeric *E. coli* FBA (average subunit surface areas for *E. coli* FBA, *E. coli* TBA, and *T. aquaticus* FBA are 16222, 12999, and 13654 Å^2, respectively). Tetrameric interface areas (645 Å^2 for *E. coli* TBA and 593 Å^2 for *T. aquaticus* FBA) are much smaller than the dimeric interface areas (1540 Å^2 for *E. coli* TBA, 1839 Å^2 for *T. aquaticus* FBA, and 2442 Å^2 for *E. coli* FBA), implying a weaker tetrameric state. These results are consistent with the findings from the experiments performed by Izard and Sygusch, who showed that the dimerization interactions are much more extensive than the tetramerization interactions.[12] Moreover, the three aldolases have almost the same ratio between the dimeric interface area and subunit area (0.15 for *E. coli* FBA, 0.13 for *E. coli* TBA, and 0.12 for *T. aquaticus* FBA).

Depicting the Catalytic Microenvironment. There is no aldolase structure in the PDB with both of the components, DHAP and GAP, bound in the catalytic pocket for *E. coli* FBA, *E. coli* TBA, or *T. aquaticus* FBA. For a clear depiction of the catalytic environment, we take substrates GAP and DHAP from 3EKZ (PDB structure for *Mycobacterium tuberculosis* class II FBA) and place them into their respective catalytic pockets in each structure of *E. coli* FBA (PDB entry 1B57), *E. coli* TBA (PDB entry 1GVF), and *T. aquaticus* FBA (PDB entry 1RVG).

DOI: 10.1021/acs.biochem.5b00042
Biochemistry 2015, 54, 3543−3554

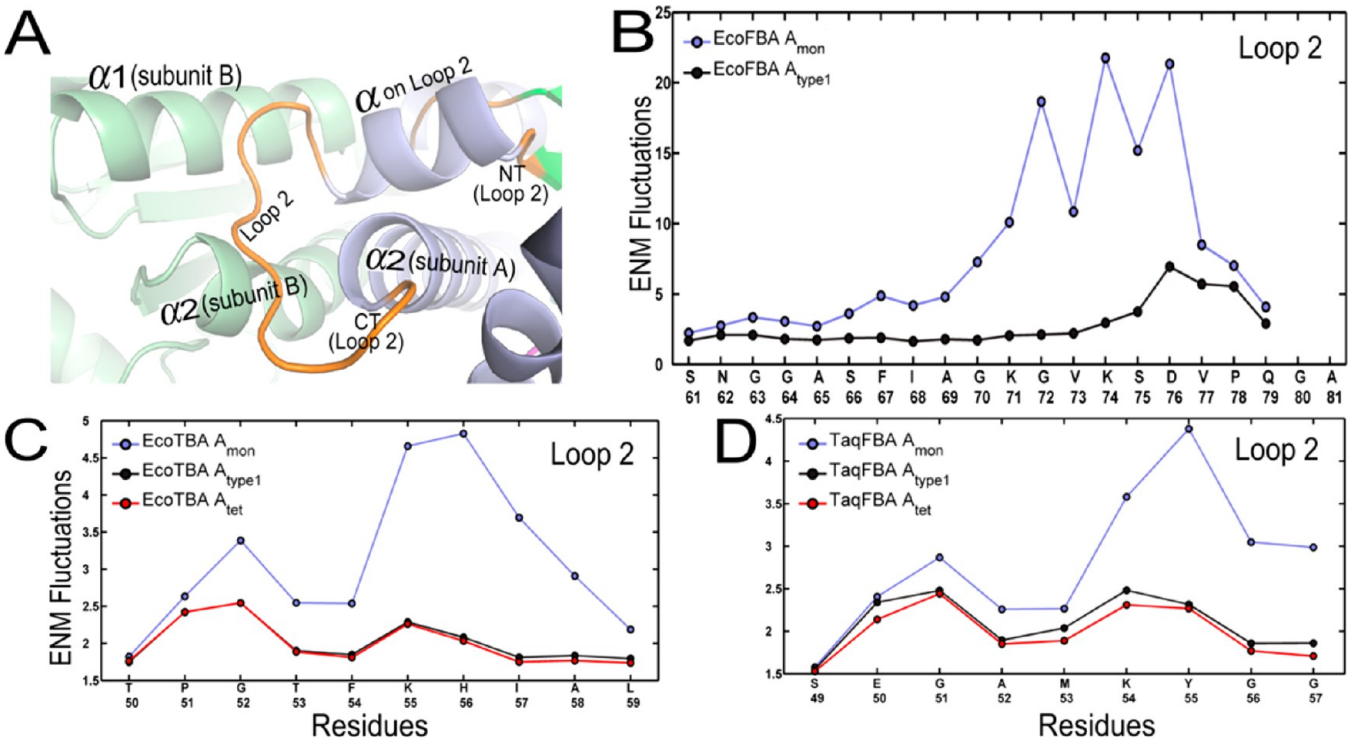

Figure 3. Computed ENM fluctuations of interface loop 2 in three aldolase structures. (A) The beamlike helical region on loop 2 of subunit A docks at the ridge between helix 1 (α1) and helix 2 (α2) of partner subunit B. (B) Fluctuations of loop 2 in the monomer (blue) and dimer (black) of the *E. coli* FBA structure. (C) Fluctuations of loop 2 in the monomer (blue), type 1 dimer (black), and tetramer (red) of *E. coli* TBA. (D) Fluctuations of loop 2 in the monomer (blue), type 1 dimer (black), and tetramer (red) of *T. aquaticus* FBA.

The rmsds (root-mean-square deviations) between one subunit of 3EKZ and one subunit of each of these structures are 0.89 Å for *E. coli* FBA, 1.46 Å for *E. coli* TBA, and 1.23 Å for *T. aquaticus* FBA. The small rmsd difference between a 3EKZ subunit and a subunit of each of the other structures gives us confidence that the placement of the substrates in the microenvironment as shown in Figures 7A and 8A is sufficiently accurate to depict the relationships between the substrates and the functional residues in the microenvironment.

Modeling Dynamics. To model the dynamics of the protein structure, we use the anisotropic network model (ANM),[20] which is a simple ENM. ENMs have been successfully used to extract the important functional motions for protein structures.[25−28] These models have further shown their abilities to study conformational transitions of macromolecules[28−30] and uncover the correlations of the global motions of proteins with the motions of the functionally important flexible loop regions.[31] Investigating the computational dynamics of some proteins such as HIV-1 protease together with its substrates and/or inhibitors using ENMs was shown to be helpful for effective inhibitor design.[32] Others utilized the ENMs to capture details of protein allosteric regulation.[33,34] The ENMs are essentially entropic models. At binding sites between protein subunits, there are many new subunit−subunit interactions upon oligomerization, corresponding to favorable energetic interactions, which we do not explicitly evaluate here. We use the term "stabilize" to refer to these new presumed-to-be-favorable interactions, where there are also reduced entropies. We intend the term "stabilize" to represent these local fluctuation changes at bound interfaces.

Here, we constructed a coarse-grained model of an aldolase structure with each residue represented by its C^{α} atom and the interaction between any two close residues represented by a spring placed between these C^{α} atoms. A spring between two residues is placed if they are within a certain cutoff distance. To model these modes of motions, there are several steps.

First, potential energy V of the system, thought to be lowest for the starting form, is taken to be harmonic and to increase as a function of the square of the displacement:

$$V = \frac{\gamma}{2}\mathbf{D}\cdot\mathbf{H}\cdot\mathbf{D}^{\mathbf{T}} \tag{1}$$

where the vector $\mathbf{D}$ is the displacement, γ is the force constant for all the springs, and $\mathbf{H}$ is the Hessian matrix containing the second derivatives of the energy function. If the structure has n residues, the Hessian matrix $\mathbf{H}$ contains $n \times n$ superelements; each element is 3×3. The ijth superelement of the Hessian matrix can be derived from the following equation:

$$H_{ij} = \begin{bmatrix} \frac{\partial^2 V}{\partial X_i\,\partial X_j} & \frac{\partial^2 V}{\partial X_i\,\partial Y_j} & \frac{\partial^2 V}{\partial X_i\,\partial Z_j} \\ \frac{\partial^2 V}{\partial Y_i\,\partial X_j} & \frac{\partial^2 V}{\partial Y_i\,\partial Y_j} & \frac{\partial^2 V}{\partial Y_i\,\partial Z_j} \\ \frac{\partial^2 V}{\partial Z_i\,\partial X_j} & \frac{\partial^2 V}{\partial Z_i\,\partial Y_j} & \frac{\partial^2 V}{\partial Z_i\,\partial Z_j} \end{bmatrix} \tag{2}$$

where X_i, Y_i, and Z_i are the positional components of residue i and V represents the harmonic potential between residues i and j. Thus, V can be expressed as follows

DOI: 10.1021/acs.biochem.5b00042
Biochemistry 2015, 54, 3543−3554

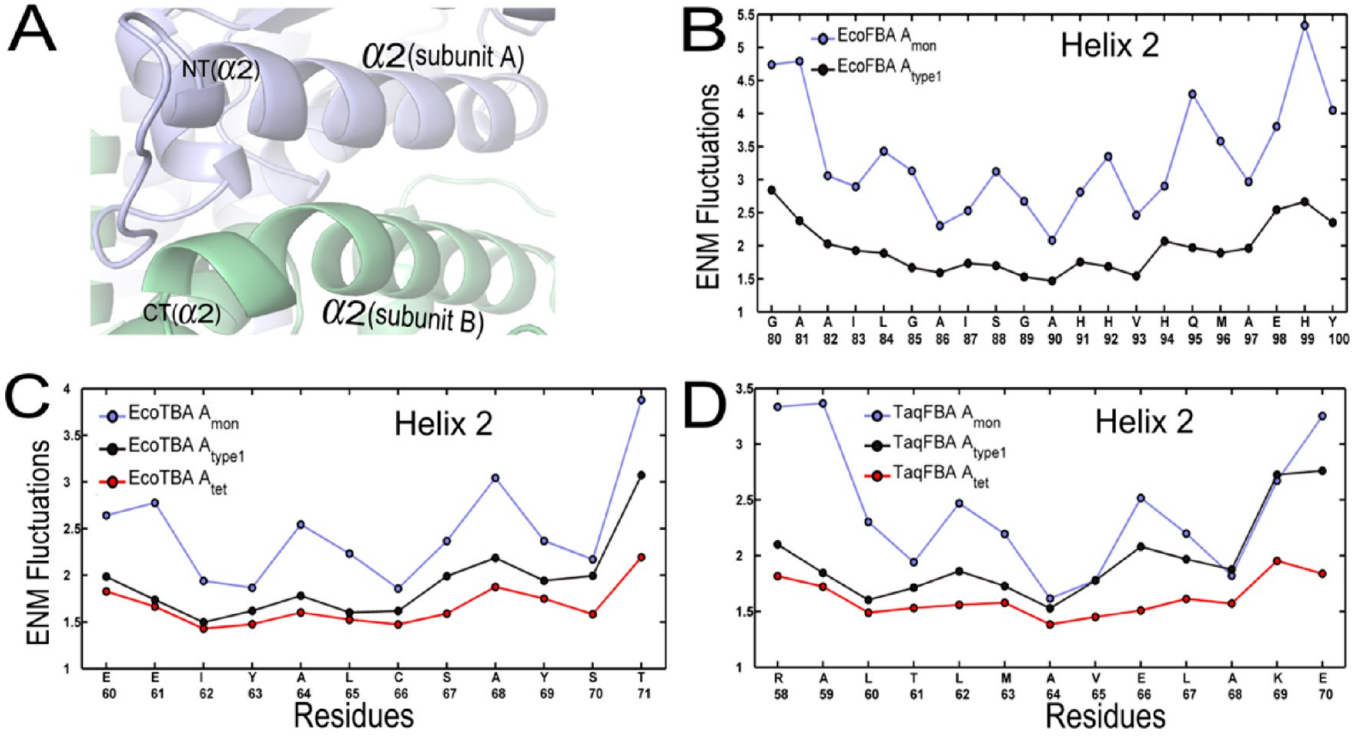

Figure 4. Computed ENM fluctuations of helix 2 (α2) in three aldolase structures. (A) Helix 2 from subunit A (blue) pairs with helix 2 from partner subunit B (green) in an antiparallel manner, based on the *E. coli* FBA structure. (B) ENM fluctuations of helix 2 in monomer (blue) and type 1 dimer (black) structures of *E. coli* FBA. (C) ENM fluctuations of helix 2 in monomer (blue), type 1 dimer (black), and tetramer (red) structures of *E. coli* TBA. (D) ENM fluctuations of helix 2 in monomer (blue), type 1 dimer (black), and tetramer (red) structures of *T. aquaticus* FBA.

$$V = \frac{\gamma}{2}(s_{ij} - s_{ij}^0)^2 = \frac{\gamma}{2}\left\{\left[(X_j - X_i)^2 + (Y_j - Y_i)^2 + (Z_j - Z_i)^2\right]^{1/2} - s_{ij}^0\right\}^2 \quad (3)$$

where s_{ij}^0 is the equilibrium distance between residues i and j. Therefore, **H** can be decomposed as follows:

$$\mathbf{H} = \mathbf{M}\cdot\mathbf{\Lambda}\cdot\mathbf{M}^{-1} \quad (4)$$

where $\mathbf{\Lambda}$ is a diagonal matrix of the eigenvalues and the columns of **M** are the eigenvectors. Each eigenvector represents one mode of motion of the structure except that the first six modes represent the rigid body translations and rotations of the structure. Thus, the fluctuations of the structure are expressed as a set of $3n - 6$ modes formed by the seventh to $3n$th eigenvector, each eigenvector giving the direction and magnitude of the corresponding mode. The eigenvalues are sorted in descending order, and each represents the importance and frequency of the corresponding mode. By comparing different ENM fluctuations with experimental *B* factors, we find that a cutoff value 13 Å is appropriate for the structures considered here.

We compute the average fluctuations of the first 50 low-frequency modes for the structures to compare their dynamics for the different structural elements.

Coupling of Motions between Structural Segments. We compute the coupling of motions for any two segments of a protein structure by first computing the normal modes of the protein structure. A normal mode describes a 3 × 1 motion vector for each residue. We normalize these 3 × 1 vectors to have unit lengths. Then we calculate the pairwise dot products of these unit vectors for the two segments of the protein structure. These dot products measure the extent of motion in the same direction, opposite direction, or orthogonal[35] to determine the extent of coupling of the motions of the residues in the two structure segments.

RESULTS

Our computations demonstrate that oligomerization through type 1 and type 2 interfaces brings stability to the structural components along these interface regions, which naturally show reduced mobilities. The computations further show that the functional components of the catalytic microenvironment achieve a catalytically competent conformation in a higher oligomeric state facilitated by aldolase global motions.

Effects of Oligomerization at the Interface Regions. *Front Loop 2.* Figure 3A shows the arrangement of loop 2 (orange) of subunit A against the ridge formed between helices 1(α1) and 2(α2) (green) from subunit B in an *E. coli* FBA structure (PDB entry 1B57). The beamlike helical region on loop 2 (identified as "α on loop 2") of subunit A docks at the ridge between helices 1 and 2 of the partner subunit B. Panels B–D show the changes in computed fluctuations for loop 2 upon oligomerization for *E. coli* FBA (PDB entry 1B57), *E. coli* TBA (PDB entry 1GVF), and *T. aquaticus* FBA (PDB entry 1RVG), respectively. The helical part and the C-terminal region of loop 2 are stabilized upon dimerization in each case. Panels C and D of Figure 3 show that tetramerization has an impact on this region much weaker than that of dimerization, stabilizing it only slightly further as shown for *E. coli* TBA and *T. aquaticus* FBA, respectively.

Helix 2. Figure 4A depicts the antiparallel arrangement of helix 2 (blue) from subunit A against helix 2 (green) from subunit B in *E. coli*. Panels B–D show the fluctuation changes

DOI: 10.1021/acs.biochem.5b00042
Biochemistry 2015, 54, 3543–3554

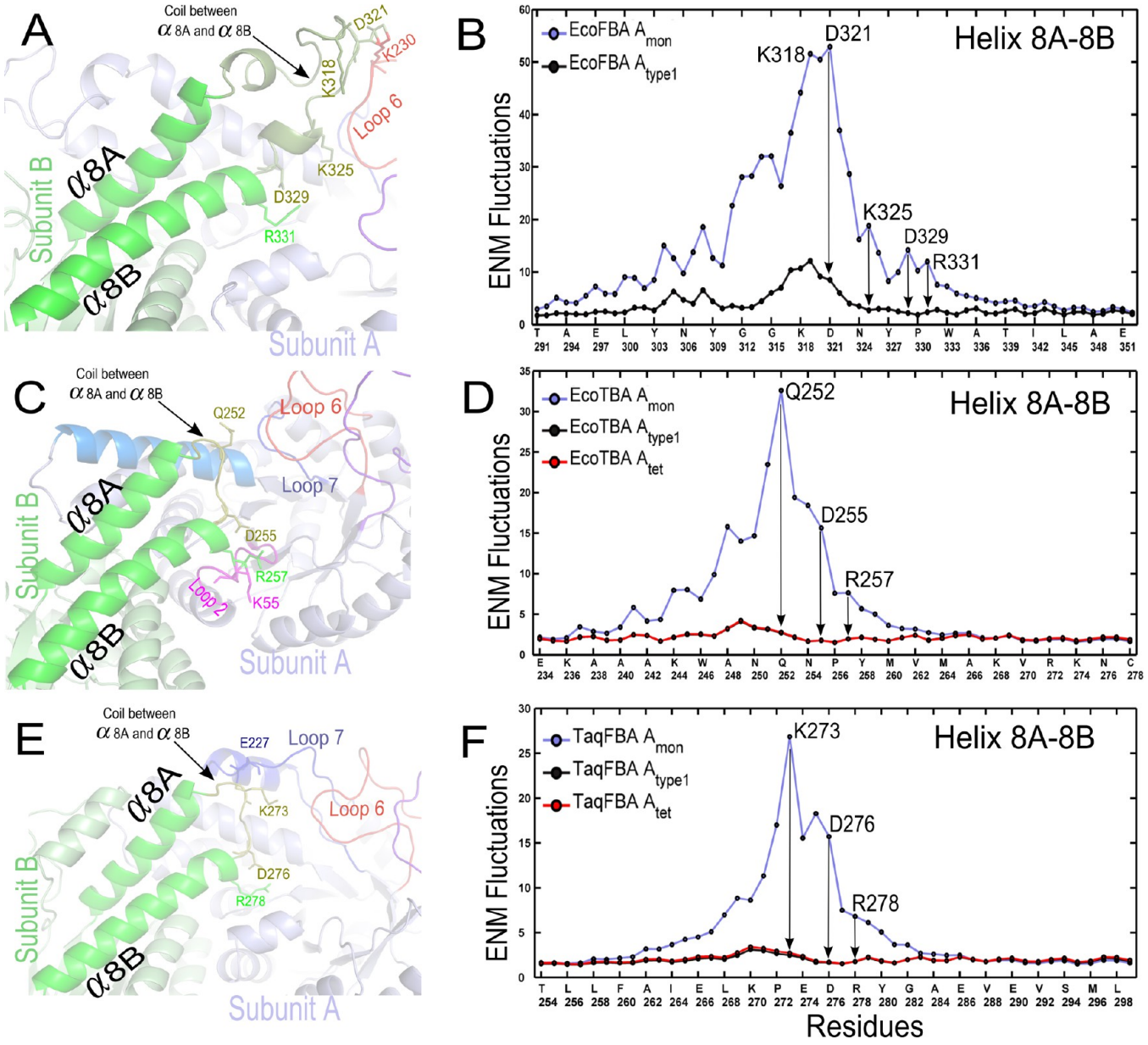

Figure 5. Computed ENM fluctuations of helix 8A (α8A), helix 8B (α8B), and the coil between them in three aldolase structures. (A) Loop 6 and the coil connecting helix 8A and helix 8B from the partner subunit in *E. coli* FBA are in the proximity of each other. K318, D321, K325, and D329 (olive green sticks) on the coil and R331 (green stick) on helix 8B are from subunit B. (B) ENM fluctuations of helices 8A and 8B and the coil between them in monomeric and type 1 dimeric structures of *E. coli* FBA. The reduction in fluctuations in loop 6 from the proximity of the coil is shown in Figure 6F. (C) The coil connecting helices 8A and 8B of one subunit and loop 6 or loop 7 from the partner subunit has a distinct spatial separation in the *E. coli* TBA structure. (D) Fluctuations of helix 8A, helix 8B, and the coil between them in monomer, type 1 dimer, and tetramer structures of *E. coli* TBA. Fluctuations of loops 6 and 7 of subunit A are shown in panels C and D of Figure 7, respectively. (E) Contact between loop 7 of subunit A and the coil connecting helices 8A and 8B of partner subunit B in *T. aquaticus* FBA. (F) Fluctuations of helices 8A and 8B and the coil between them in monomer, type 1 dimer, and tetramer structures of *T. aquaticus* FBA. The change in the fluctuations of loop 7 making contact with the coil from the partner subunit is shown in Figure 8D.

along this region upon oligomerization in *E. coli* FBA, *E. coli* TBA, and *T. aquaticus* FBA, respectively. Dimerization stabilizes the motion of this region in each case by reducing the fluctuations. Tetramerization in *E. coli* TBA and *T. aquaticus* FBA further reduces the fluctuations (panels C and D of Figure 4, respectively). This suggests that formation of a tetramer through the interactions by the type 2 interface reduces the fluctuations along this region allosterically. Because of the reduced fluctuations in the helix 2 region, tetramerization brings further stability to the aldolase tetrameric configuration.

Helix 8A Connected via a Coil to Helix 8B. Helices 8A and 8B participate in the formation of the dimerization interface, and the coil connecting them can come into the proximity of the functional loops of the partner subunit. Figure 5A shows such organization formed in an *E. coli* FBA structure. The proximity of loop 6 and the coil connecting helix 8A and helix 8B from the partner subunit brings residues K318 (on the coil) and D321 (on loop 6) into close contact. K318, D321, K325, and D328 (olive green sticks) on the coil and R331 (green stick) on helix 8B are from subunit B and play roles in the

DOI: 10.1021/acs.biochem.5b00042
Biochemistry 2015, 54, 3543−3554

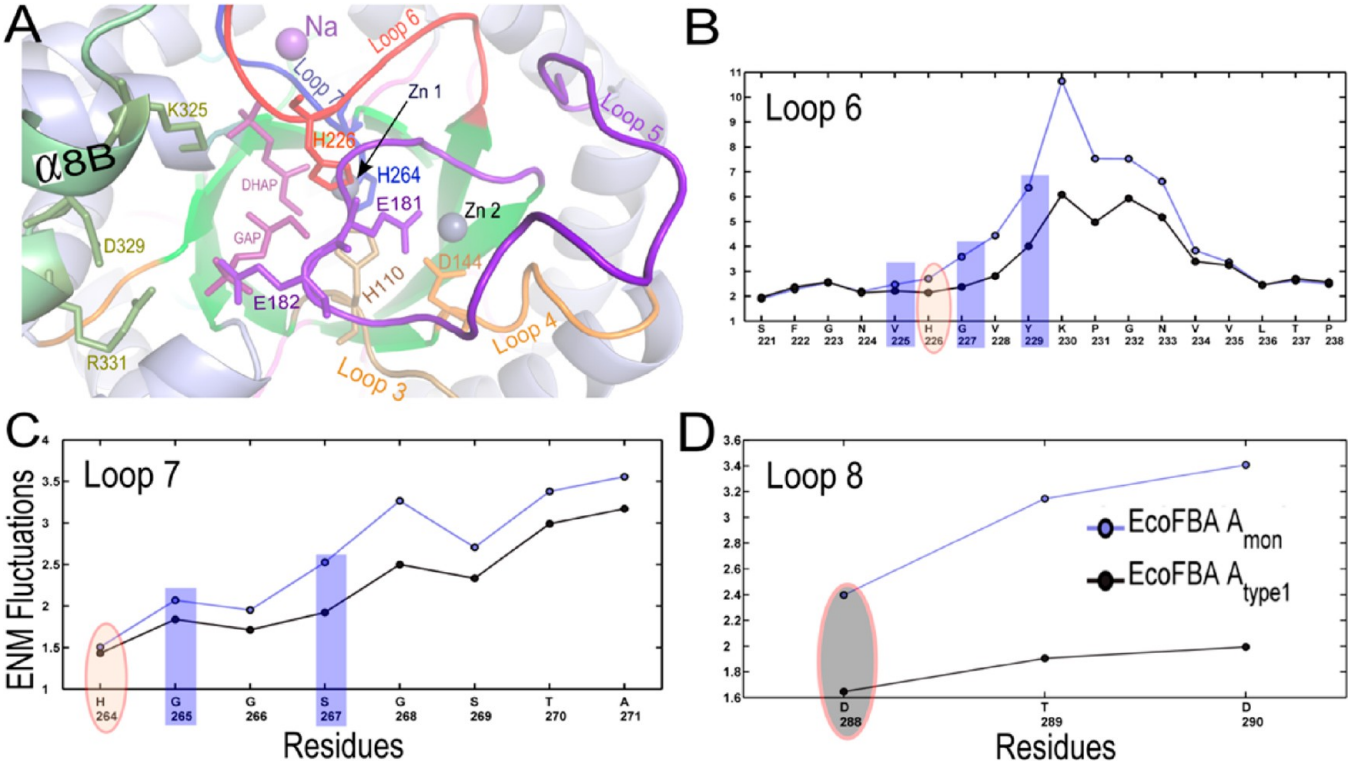

Figure 6. Comparing ENM fluctuations of the functional loops in *E. coli* fructose 1,6-bisphosphate aldolase (FBA) monomeric and dimeric structures. (A) Functional loops 3−7 surround the catalytic pocket. The proximity between loop 6 of subunit A (blue) and the coil between helix 8A and helix 8B from subunit B (green) is greatest between K230 (red stick) on loop 6 and D321 (green stick) on the coil. (B) Fluctuations of loop 6 in the monomer and dimer. (C) Fluctuations of loop 7 in the monomer and dimer. (D) Fluctuations of loop 8 in the monomer and dimer. On the ENM fluctuation curves, the substrate binding residues are shown with a gray oval, Zn^{2+} ion binding residues are marked with orange ovals, and Na^{+} binding residues are marked with blue rectangles.

catalytic environment in subunit A. D321, located on the coil, comes into close contact with K230 (olive stick) on loop 6 of subunit A. K325, D329, and R331 are three catalytically important residues from subunit B that contribute to the formation of the catalytic environment in subunit A. Figure 5B demonstrates the change in fluctuations along helices 8A and 8B, and their connecting coil. Aldolase dimerization in *E. coli* FBA stabilizes the motions of these components.

Figure 5C shows the arrangement of loop 6 and loop 7 of one subunit and the coil connecting helices 8A and 8B of the partner subunit in *E. coli* TBA. In this arrangement, the coil and all loops are further apart than in *E. coli* FBA. Q252 (olive stick) on the coil between helix 8A and helix 8B of subunit B makes contact with helix 8A of subunit A. D255 (olive green stick) and R257 (green stick) from subunit B play a role in the formation of the catalytic environment in subunit A. R257 makes contact with K55 as magenta sticks on loop 2 of subunit A. Figure 5D demonstrates the change in fluctuations of helix 8A, helix 8B, and the coil between them in monomer, type 1 dimer, and tetramer structures of *E. coli* TBA. Dimerization stabilizes this region as in *E. coli* FBA, and tetramerization does not have a significant further effect on their motions.

Figure 5E shows the contact between loop 7 of subunit A and the coil connecting helix 8A and helix 8B of partner subunit B in *T. aquaticus* FBA. K273 (olive green stick) on the coil makes contact with E227 (blue stick) on loop 7. D276 (olive green stick) and R278 (green stick) are two other important residues of subunit B that contribute to the formation of the catalytic environment in subunit A. The change in fluctuations of helices 8A and 8B and their connecting coil region in monomer, type 1 dimer, and tetramer structures are shown in Figure 5F. Similar to the case in *E. coli* TBA, dimerization stabilizes this region to the fullest and tetramerization does not have a significant effect.

Effects of Oligomerization at the Catalytic Microenvironment. *Dynamics of the E. coli FBA Catalytic Environment.* The major structural components contributing to the formation and dynamics of the catalytic microenvironment are loops 3−7 from one subunit in association with helix 8B from the partner subunit. Oligomerization changes the dynamics of these components, making the structure suitable for catalytic activity.

Figure 6A shows the arrangement of functional loops 3−7 and the substrates DHAP and GAP in the catalytic pocket in subunit A of *E. coli* FBA. The coil between helix 8A and helix 8B from the partner subunit approaches loop 6. Residues K325, D329, and R331 on helix 8B from the partner subunit also contribute to the formation of the environment. Figure 6A shows an enlarged view of the catalytic pocket. H110 (dark gray stick) on loop 4, H226 (red stick) on loop 6, and H264 (blue stick) on loop 7, together with the substrate and/or product, function as ligands for Zn^{2+}, shown as gray spheres Zn1 and Zn2. Residue D144 (orange stick) on loop 4 functions as one of the ligands for the cation in the open state of the structure. E181 and E182 (purple sticks) are two catalytically important residues on loop 5. K325, D329, and R331 (green sticks) on helix 8B from partner subunit B contribute to the construction of the catalytic pocket in subunit A. Two substrates and/or products DHAP and GAP are shown as purple sticks in the catalytic pocket.

DOI: 10.1021/acs.biochem.5b00042
Biochemistry 2015, 54, 3543−3554

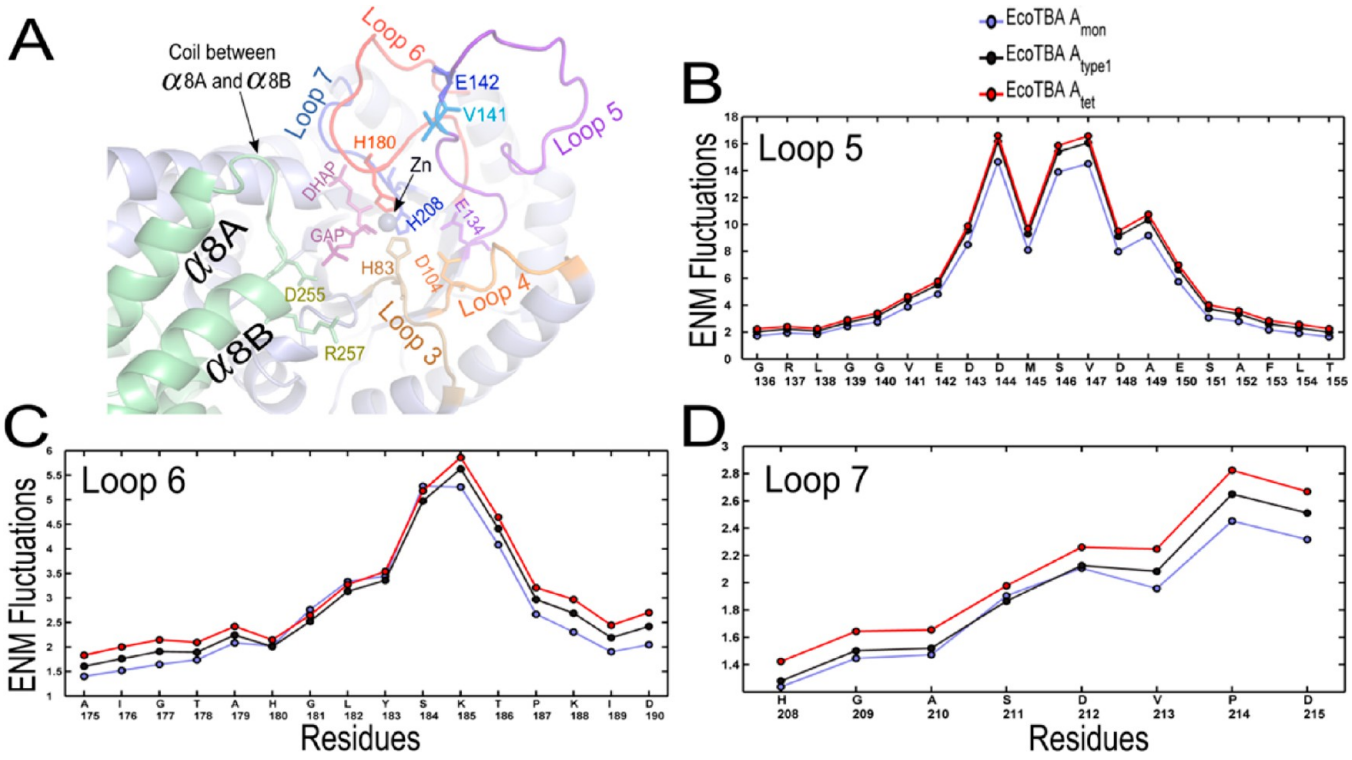

Figure 7. Changes in the computed ENM fluctuations of functional loops 5−7 in *E. coli* tagatose 1,6-bisphosphate aldolase (TBA) upon oligomerization. (A) Catalytic pocket and its important components. (B) Fluctuations of loop 5 in monomer, type 1 dimer, and tetramer structures. (C) Fluctuations of loop 6 in monomer, type 1 dimer, and tetramer structures. (D) Fluctuations of loop 7 in monomer, type 1 dimer, and tetramer structures.

Panels B−D of Figure 6 show the change in the computed fluctuations of functional loops 6−8, respectively, upon oligomerization. It is evident that dimerization reduces the extents of loop motion in each case. Consequently, the catalytically important residues on these loops achieve their optimal mobility. For example, appropriate interplay of the two cations, divalent Zn^{2+} and monovalent Na^{+}, is essential for aldolase catalysis.[9] Hall et al. have shown experimentally that Zn^{2+} binding ligand residues in the *E. coli* aldolase structure are H110 (on loop 3), H226 (on loop 6), H264 (on loop 7), and D144.[11] In accord with their findings, our results show that dimerization stabilizes these residues, which may facilitate the proper positioning of the residues in the catalytic pocket. Moreover, Na^{+} binding scaffold residues are V225, G227, Y229 (on loop 6), and G265 and S267 (on loop 7) and their appropriate motions help the interplay between Na^{+} and Zn^{2+}, facilitating the catalytic mechanism.[9] Our simulations further show that dimerization stabilizes these residues (blue rectangles in Figure 6B,C). D109 (on loop 3), E182 (on loop 5), and D288 (on loop 8) were previously found to be three of the residues essential for catalysis.[15,17] Our computations are consistent with the previous experimental results of Pegan et al., who showed that appropriate loop dynamics are essential for their functioning.[16] Our simulations show that dimerization stabilizes these residues. Figure 6D shows the change in fluctuation in D288 (shaded oval) upon dimerization.

Dynamics of the E. coli TBA Catalytic Environment. Figure 7A shows the arrangement of the catalytically important loops, residues, and substrates in an *E. coli* TBA. Functional loops 3 (dark gray), 4 (orange), 5 (purple), 6 (red), and 7 (blue) surround the catalytic pocket. Catalytic products DHAP and GAP are shown as purple sticks in the catalytic pocket. H83 (gray stick) on loop 3, H180 (red stick) on loop 6, and H208 (blue stick) on loop 7 are the three histidine ligands for Zn^{2+} (gray spheres) in the closed state of the structure. D104 (orange stick) on loop 4 is a cation binding residue in the open state of the structure. E134 (purple stick), V141 (marine blue stick), and E142 (dark blue stick) are three catalytically important residues on loop 5. E142 also binds with the substrate and/or product. There is no contact between loop 6 or loop 7 and the coil connecting helix 8A and helix 8B. The pocket is in an open conformation, and functional Loop 5 is away from the center of the pocket.

Panels B−D of Figure 7 show the computed fluctuations of loops 5−7, respectively, in different oligomeric states. In each case, oligomerization has slightly increased the fluctuations.

Figure 7A shows the microenvironment of the catalytic pocket of *E. coli* TBA. It is evident from this figure that the shortened coil between helices 8A and 8B of the partner subunit is unable to make close contact with functional loop 6 or 7. The consequence of this architectural difference with *T. aquaticus* FBA is that oligomerization increases the fluctuations of all functional loops there. However, the catalytically conserved residues maintain a similar spatial arrangement. The distance between D255 (atom OD2) and GAP (atom N) is 2.4 Å, and the distance between R257 (atom O2P) and GAP (atom N) is 7.4 Å. Catalytically important residues V141 and E142 are on loop 5. The Zn^{2+} ion is held by H83, H180, H208, and the substrate. D104 (on loop 4) and E134 (on loop 5) function as ligands for Zn^{2+} in the open conformation.

Figure 5C shows the proximity of loop 7 of subunit A to the coil from subunit B in the tetrameric *E. coli* TBA. D255 and R257 on helix 8B from subunit B are important for the formation of the catalytic pocket in subunit A. Q252 on the coil

DOI: 10.1021/acs.biochem.5b00042
Biochemistry 2015, 54, 3543−3554

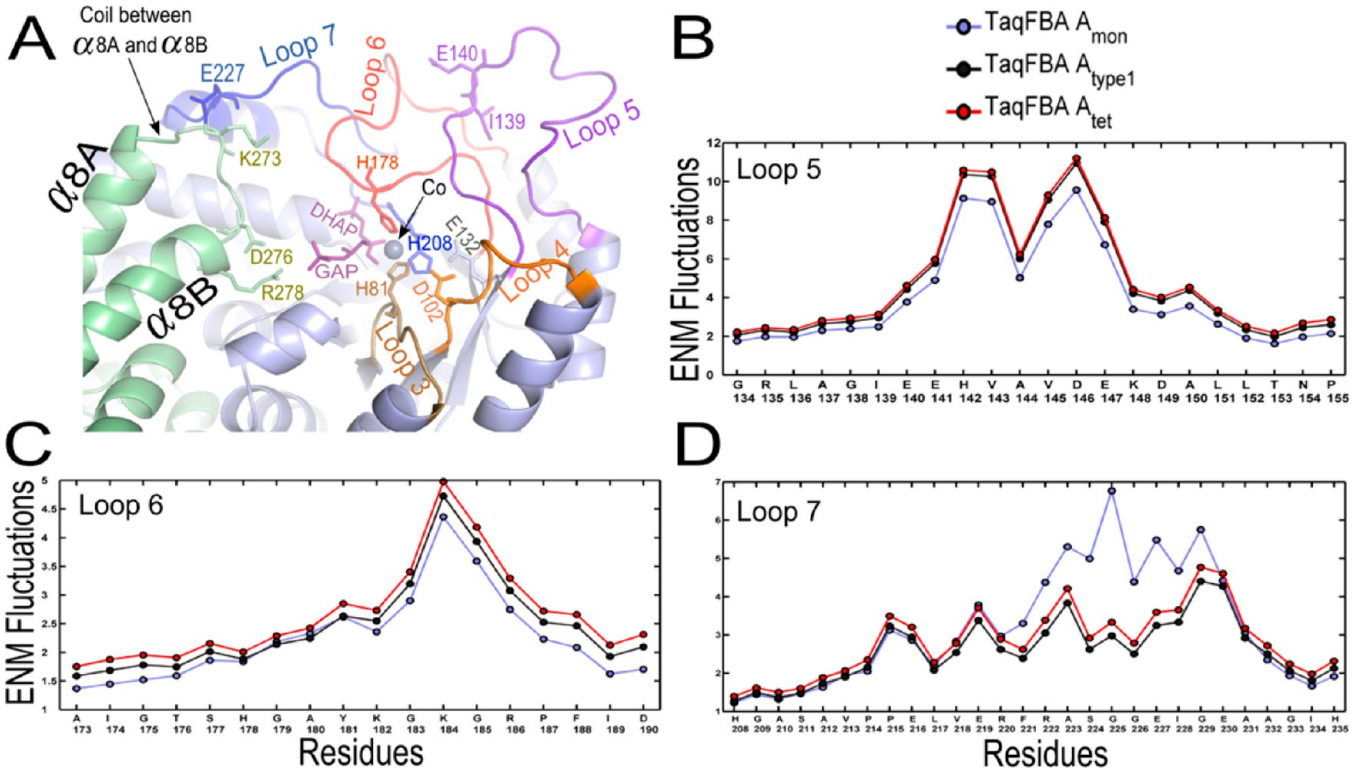

Figure 8. Changes in the computed ENM fluctuations of loops 5−7 in *T. aquaticus* fructose 1,6-bisphosphate aldolase (FBA) (PDB entry 1RVG) upon oligomerization. (A) Catalytic pocket and its important components of *T. aquaticus* FBA. (B) Fluctuations of loop 5 in monomer, type 1 dimer, and tetramer structures. (C) Fluctuations of loop 6 in monomer, type 1 dimer, and tetramer structures. (D) Fluctuations of loop 7 in monomer, type 1 dimer, and tetramer structures.

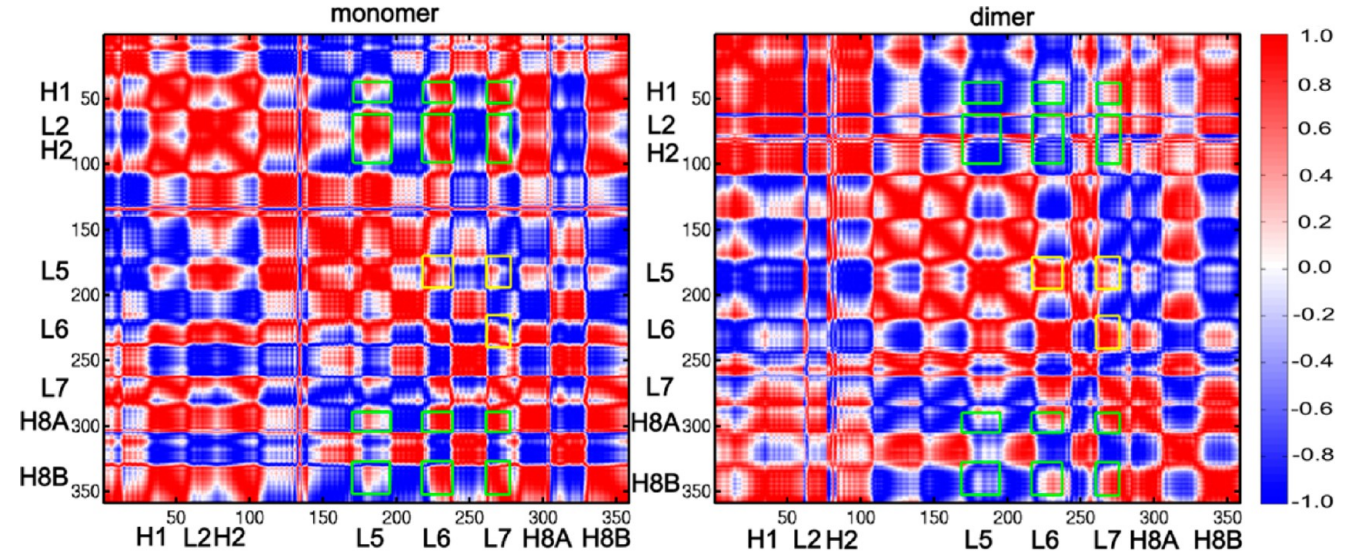

Figure 9. Heat map showing the correlations between the interfacial region and the functional loops in monomeric (left) and dimeric (right) subunits (chain A vs chain A) of *E. coli* FBA. Dimeric interface-forming regions are labeled as H1 (helix 1), L2 (loop 2), H2 (helix 2), H8A (helix 8A), and H8B (helix 8B). Functional loops are labeled as L5 (loop 5), L6 (loop 6), and L7 (loop 7). Dimerization modifies the correlation between these structural components. The correlation between H1 and L5 changes from being almost positive to totally negative. Correlations between H1 and {L6, L7} shift from being strongly positive to mostly positive. Correlations between {L2, H2} and {L5, L6, L7} show similar patterns. {H8A, H8B} and L5 shift from being loosely coupled to being strongly anticorrelated. The correlation between {H8A, H8B} and L6 shifts from being strongly positive to less positive. Strong correlation between {H8A, H8B} and L6 remains almost the same in the dimeric subunit, as well. The correlation between L5 and L6 shifts from being less positive to more positive; the coupling between L5 and L7 shifts from being almost anticorrelated to being mostly positively correlated. The correlation between L6 and L7 changes from being less positive to more positive. Colors: green rectangle, correlation between an interfacial region and a functional loop; yellow rectangle, correlation between functional loop pairs.

region of subunit B approaches loop 7 from subunit A. Figure 5D shows how the computed fluctuations of helices 8A and 8B and the coil between them change upon oligomerization. Dimerization stabilizes this region the most, and tetrameriza-

DOI: 10.1021/acs.biochem.5b00042
Biochemistry 2015, 54, 3543−3554

tion has relatively little effect on the computed fluctuations. The structural organization of the catalytic pocket in tetrameric *E. coli* TBA differs from that of *E. coli* FBA or *T. aquaticus* FBA in such a way that none of the functional loops from one subunit come into close contact with any part of the partner subunit.

Dynamics of the T. aquaticus FBA Catalytic Environment. Figure 8A shows the catalytic pocket of tetrameric *T. aquaticus* FBA. Functional loops 3 (dark gray), 4 (orange), 5 (purple), 6 (red), and 7 (blue) surround the catalytic pocket. H81 (dark gray stick) on loop 3, H178 (red stick) on loop 6, and H208 (blue stick) on loop 7 function as ligands for divalent cation Co^{2+} (gray sphere) in the closed state of the structure. D102 (orange stick) on loop 4 is a cation binding residue in the open state of the structure. E227 (blue stick) on loop 7 comes into close contact with K273 (green stick) on the coil between helices 8A and 8B of the partner subunit. Two more catalytically important residues D276 and R278 (green sticks) from artner subunit B contribute to the catalytic pocket in subunit A. DHAP and GAP are shown as purple sticks in the catalytic pocket. E132 (gray stick), I139 (purple stick), and E140 (purple stick) are three catalytically significant residues on loop 5. E140 plays a role in substrate binding, as well.

Panels B–D of Figure 8 show the changes in the computed fluctuations upon oligomerization for functional loops 5–7, respectively. It is important to note that loop 7 approaches the coil between helices 8A and 8B of the partner subunit; the residues making the close contacts are labeled in Figure 8A: E227 from loop 7 and K273 from the coil. This suppresses the motions of loop 7 as shown in Figure 8D. This also attenuates the mobility of D276 and R278, two of the substrate binding residues from the partner subunit. The computed fluctuations along the other two functional loops, 5 and 6, increase upon dimerization as shown in panels B and C of Figure 8, respectively. Tetramerization does not increase the fluctuations as much in comparison with the changes effected by dimerization.

Figure 5E shows the proximity of loop 7 and the coil between helices 8A and 8B of the partner subunit in the *T. aquaticus* FBA tetrameric structure. D276 and R278 on helix 8B of subunit B are important for the catalytic pocket in the partner subunit A. K273 on the coil closely approaches loop 7 of subunit A. Figure 5F shows how the computed fluctuation changes upon oligomerization along helices 8A and 8B and the coil between them. It is clear that dimerization attenuates the computed fluctuations the most along this region and that tetramerization has a much weaker effect. Figure 8A shows another view of this region of the structure in Figure 5E but emphasizes more the structural components of the catalytic microenvironment, comprising the components from both subunits (A and B) joined by a type 1 interface.

Dynamic Coupling between the Subunit Interfacial Region and Functional Loops. The coupling between the subunit interfacial region and the functional loops changes upon aldolase oligomerization. The correlations between the interfacial region and the functional loops in *E. coli* FBA are shown in Figure 9 (left panel, monomeric subunit; right panel, dimeric subunit). The residues in helix 1 and those in loop 5 move in a strongly positive correlated way in the monomeric unit, whereas they move in a strongly anticorrelated way in the dimeric subunit. Helix 1 and loop 6 shift to be loosely coupled in the dimeric subunit. The correlation between helix 1 and loop 7 residues also changes from strongly positive to less positive. Further, the coupling of the movements of the residues in helices 8A and 8B with those in loop 5 changes from loosely coupled to strongly anticorrelated. The correlations of the residues in these helices with loops 6 and 7 remain highly coupled in the dimeric subunit. Overall, these observations reveal a significant shift in the dynamic coupling between the interfacial region and the functional loops upon dimerization. Moreover, the correlation between the functional loops (loop 5 vs loop 6, loop 5 vs loop 7, and loop 6 vs loop 7) shifts to be strongly positive in the dimeric structure. Additionally, in the case of *E. coli* TBA and *T. aquaticus* FBA, the interfacial region and the functional loops are shown to have a strong positive correlation or a strong anticorrelation, predominantly. From these observations, we can surmise that the functional oligomeric states of these aldolases show a stronger coupling of the motions between the intersubunit interfaces and the functional loops.

DISCUSSION

In summary, our normal-mode analyses of the three aldolase structures confirm what was previously known about the aldolase loop dynamics. We further demonstrate that the functional loop dynamics change upon oligomerization to facilitate the catalytic mechanism. We also find that the motions of the aldolase oligomerization interfaces stabilize upon higher-order oligomerization.

Our computations show that aldolase oligomerization changes the functional loop motions. On *E. coli* FBA with longer functional loops 5–7, oligomerization decreases the magnitudes of their motions, making them suitable for a catalytic mechanism. On the other hand, on *E. coli* TBA and *T. aquaticus* FBA that have shorter functional loops, oligomerization increases the extents of motion of those loops. This implies that oligomerization allows the aldolase structures to achieve suitable dynamics of the loops contributing to the formation of the catalytic microenvironment. This is consistent with the previous findings showing the importance of maintaining catalytic motions for loop 5[15] and loops 3 and 8.[17]

Loop 2, helix 2, and helices 8A and 8B are the components that form the oligomeric interfaces. Oligomerization reduces the fluctuations of these regions by bringing the structure to an energetically more favorable state. This is consistent with the previous findings of Miteva et al., who showed that higher-order oligomeric aldolase states are energetically more stable than the monomeric forms.[19] Further, the stabilization of helices 8A and 8B through oligomerization reduces the mobility of these regions as required, to allow the catalytic residues on these segments (K325 and R331 in *E. coli* FBA, D255 and R257 in *E. coli* TBA, and D276 and R278 in *T. aquaticus* FBA) to contribute to the catalytic process. This supports the previous finding of Zgiby et al., who showed the importance of a stable K325 in *E. coli* catalysis,[11] and the result of Qamar et al., who showed the stability of R331 in substrate binding.[13] In addition, computations show that functionally active higher-order oligomeric states exhibit stronger coupling of motions between the intersubunit interfacial region and the functional loops, in each of the aldolase structures.

Our conclusions about the three representative class II aldolases, *E. coli* FBA, *E. coli* TBA, and *T. aquaticus* FBA, are that these aldolases have similar catalytic microenvironments. They differ in their functional loop lengths. *E. coli* FBA has longer functional loops. In particular, loops 5 and 6 are much longer than the loops on more compact structures of *E. coli*

DOI: 10.1021/acs.biochem.5b00042
Biochemistry 2015, 54, 3543–3554

TBA and *T. aquaticus* FBA. Because of the slightly different oligomeric architectures of these aldolase structures, the *E. coli* FBA global motions decrease the extents of functional loop motion after oligomerization, whereas oligomerization in *E. coli* TBA and *T. aquaticus* FBA increases the dynamics of the corresponding shorter functional loops. We suggest that the modified dynamics and the stronger couplings between the intersubunit interfacial region and the functional loops in the higher-order oligomeric states of the aldolases help them realize catalytic competency. The approaches taken here by coarse-graining the structures have allowed us to establish direct connections with a large range of experimental results and uncover many details relating to catalysis in these enzymes.

■ ASSOCIATED CONTENT

Supporting Information

Organization of higher-order oligomeric structures of aldolases, depiction of type 1 and type 2 interfaces, coupling of motions between the subunit interface and the functional loops in two tetrameric structures, and a table listing the conserved binding and catalytic residues in aldolases. The Supporting Information is available free of charge on the ACS Publications website at DOI: 10.1021/acs.biochem.5b00042.

■ AUTHOR INFORMATION

Corresponding Author

*E-mail: jernigan@iastate.edu.

Present Address

†A.R.K.: Laboratory of Cell Biology, Building 37, Room 3035, National Cancer Institute, CCR, NIH, 37 Convent Dr., Bethesda, MD 20892-4258. Phone: (301) 451-7844. E-mail: ataur.katebi@mail.nih.gov.

Author Contributions

A.R.K. and R.L.J. both contributed to the design, execution, and writing of this work.

Funding

This research was supported by National Science Foundation Grant MCB-1021785 and National Institutes of Health Grant R01GM072014.

Notes

The authors declare no competing financial interest.

■ ACKNOWLEDGMENTS

We thank the National Institutes of Health Fellows Editorial Board for reviewing the manuscript.

■ REFERENCES

(1) Morse, D. E., and Horecker, B. L. (1968) The mechanism of action of aldolases. *Adv. Enzymol. Relat. Areas Mol. Biol. 31*, 125−181.

(2) Lorentzen, E., Siebers, B., Hensel, R., and Pohl, E. (2005) Mechanism of the Schiff base forming fructose-1,6-bisphosphate aldolase: Structural analysis of reaction intermediates. *Biochemistry 44*, 4222−4229.

(3) Rutter, W. J. (1964) Evolution of aldolase. *Fed. Proc. 23*, 1248−1257.

(4) Galkin, A., Li, Z., Li, L., Kulakova, L., Pal, L. R., Dunaway-Mariano, D., and Herzberg, O. (2009) Structural insights into the substrate binding and stereoselectivity of *Giardia* fructose-1,6-bisphosphate aldolase. *Biochemistry 48*, 3186−3196.

(5) Hall, D. R., Kemp, L. E., Leonard, G. A., Marshall, K., Berry, A., and Hunter, W. N. (2003) The organization of divalent cations in the active site of cadmium *Escherichia coli* fructose-1,6-bisphosphate aldolase. *Acta Crystallogr. D59*, 611−614.

(6) Li, Z., Liu, Z., Cho, D. W., Zou, J., Gong, M., Breece, R. M., Galkin, A., Li, L., Zhao, H., Maestas, G. D., Tierney, D. L., Herzberg, O., Dunaway-Mariano, D., and Mariano, P. S. (2011) Rational design, synthesis and evaluation of first generation inhibitors of the *Giardia lamblia* fructose-1,6-biphosphate aldolase. *J. Inorg. Biochem. 105*, 509−517.

(7) Richards, O. C., and Rutter, W. J. (1961) Preparation and properties of yeast aldolase. *J. Biol. Chem. 236*, 3177−3184.

(8) Richards, O. C., and Rutter, W. J. (1961) Comparative properties of yeast and muscle aldolase. *J. Biol. Chem. 236*, 3185−3192.

(9) Hall, D. R., Leonard, G. A., Reed, C. D., Watt, C. I., Berry, A., and Hunter, W. N. (1999) The crystal structure of *Escherichia coli* class II fructose-1,6-bisphosphate aldolase in complex with phosphoglycolohydroxamate reveals details of mechanism and specificity. *J. Mol. Biol. 287*, 383−394.

(10) Hall, D. R., Bond, C. S., Leonard, G. A., Watt, C. I., Berry, A., and Hunter, W. N. (2002) Structure of tagatose-1,6-bisphosphate aldolase. Insight into chiral discrimination, mechanism, and specificity of class II aldolases. *J. Biol. Chem. 277*, 22018−22024.

(11) Zgiby, S. M., Thomson, G. J., Qamar, S., and Berry, A. (2000) Exploring substrate binding and discrimination in fructose 1,6-bisphosphate and tagatose 1,6-bisphosphate aldolases. *Eur. J. Biochem. 267*, 1858−1868.

(12) Izard, T., and Sygusch, J. (2004) Induced fit movements and metal cofactor selectivity of class II aldolases: Structure of *Thermus aquaticus* fructose-1,6-bisphosphate aldolase. *J. Biol. Chem. 279*, 11825−11833.

(13) Qamar, S., Marsh, K., and Berry, A. (1996) Identification of arginine 331 as an important active site residue in the class II fructose-1,6-bisphosphate aldolase of *Escherichia coli*. *Protein Sci. 5*, 154−161.

(14) Cooper, S. J., Leonard, G. A., McSweeney, S. M., Thompson, A. W., Naismith, J. H., Qamar, S., Plater, A., Berry, A., and Hunter, W. N. (1996) The crystal structure of a class II fructose-1,6-bisphosphate aldolase shows a novel binuclear metal-binding active site embedded in a familiar fold. *Structure 4*, 1303−1315.

(15) Zgiby, S., Plater, A. R., Bates, M. A., Thomson, G. J., and Berry, A. (2002) A functional role for a flexible loop containing Glu182 in the class II fructose-1,6-bisphosphate aldolase from *Escherichia coli*. *J. Mol. Biol. 315*, 131−140.

(16) Pegan, S. D., Rukseree, K., Capodagli, G. C., Baker, E. A., Krasnykh, O., Franzblau, S. G., and Mesecar, A. D. (2013) Active site loop dynamics of a class IIa fructose 1,6-bisphosphate aldolase from *Mycobacterium tuberculosis*. *Biochemistry 52*, 912−925.

(17) Plater, A. R., Zgiby, S. M., Thomson, G. J., Qamar, S., Wharton, C. W., and Berry, A. (1999) Conserved residues in the mechanism of the *E. coli* Class II FBP-aldolase. *J. Mol. Biol. 285*, 843−855.

(18) Pezza, J. A., Stopa, J. D., Brunyak, E. M., Allen, K. N., and Tolan, D. R. (2007) Thermodynamic analysis shows conformational coupling and dynamics confer substrate specificity in fructose-1,6-bisphosphate aldolase. *Biochemistry 46*, 13010−13018.

(19) Miteva, M., Alexov, E., and Atanasov, B. (1998) Numerical simulation of aldolase tetramer stability. *Eur. Biophys. J. 28*, 67−73.

(20) Atilgan, A. R., Durell, S. R., Jernigan, R. L., Demirel, M. C., Keskin, O., and Bahar, I. (2001) Anisotropy of fluctuation dynamics of proteins with an elastic network model. *Biophys. J. 80*, 505−515.

(21) Alefounder, P. R., Baldwin, S. A., Perham, R. N., and Short, N. J. (1989) Cloning, sequence analysis and over-expression of the gene for the class II fructose 1,6-bisphosphate aldolase of *Escherichia coli*. *Biochem. J. 257*, 529−534.

(22) Eyrisch, O., Sinerius, G., and Fessner, W. (1993) Facile enzymic de novo synthesis and NMR spectroscopic characterization of D-tagatose 1,6-bisphosphate. *Carbohydr. Res. 238*, 287−306.

(23) Ashkenazy, H., Erez, E., Martz, E., Pupko, T., and Ben-Tal, N. (2010) ConSurf 2010: Calculating evolutionary conservation in sequence and structure of proteins and nucleic acids. *Nucleic Acids Res. 38*, W529−W533.

(24) Krissinel, E., and Henrick, K. (2007) Inference of macromolecular assemblies from crystalline state. *J. Mol. Biol. 372*, 774−797.

DOI: 10.1021/acs.biochem.5b00042
Biochemistry 2015, 54, 3543−3554

(25) Bahar, I., Erman, B., Haliloglu, T., and Jernigan, R. L. (1997) Efficient characterization of collective motions and interresidue correlations in proteins by low-resolution simulations. *Biochemistry 36*, 13512−13523.
(26) Bahar, I., Atilgan, A. R., and Erman, B. (1997) Direct evaluation of thermal fluctuations in proteins using a single-parameter harmonic potential. *Folding Des. 2*, 173−181.
(27) Doruker, P., Jernigan, R. L., and Bahar, I. (2002) Dynamics of large proteins through hierarchical levels of coarse-grained structures. *J. Comput. Chem. 23*, 119−127.
(28) Leioatts, N., Romo, T. D., and Grossfield, A. (2012) Elastic Network Models are Robust to Variations in Formalism. *J. Chem. Theory Comput. 8*, 2424−2434.
(29) Deriu, M. A., Soncini, M., Orsi, M., Patel, M., Essex, J. W., Montevecchi, F. M., and Redaelli, A. (2010) Anisotropic elastic network modeling of entire microtubules. *Biophys. J. 99*, 2190−2199.
(30) Mao, Y. (2011) Dynamical basis for drug resistance of HIV-1 protease. *BMC Struct. Biol. 11*, 31.
(31) Kurkcuoglu, Z., Bakan, A., Kocaman, D., Bahar, I., and Doruker, P. (2012) Coupling between catalytic loop motions and enzyme global dynamics. *PLoS Comput. Biol. 8*, e1002705.
(32) Ozer, N., Schiffer, C. A., and Haliloglu, T. (2010) Rationale for more diverse inhibitors in competition with substrates in HIV-1 protease. *Biophys. J. 99*, 1650−1659.
(33) Giardina, G., Paiardini, A., Fernicola, S., Franceschini, S., Rinaldo, S., Stelitano, V., and Cutruzzola, F. (2013) Investigating the allosteric regulation of YfiN from *Pseudomonas aeruginosa*: Clues from the structure of the catalytic domain. *PLoS One 8*, e81324.
(34) Rodgers, T. L., Townsend, P. D., Burnell, D., Jones, M. L., Richards, S. A., McLeish, T. C., Pohl, E., Wilson, M. R., and Cann, M. J. (2013) Modulation of global low-frequency motions underlies allosteric regulation: Demonstration in CRP/FNR family transcription factors. *PLoS Biol. 11*, e1001651.
(35) Zimmermann, M. T., Kloczkowski, A., and Jernigan, R. L. (2011) MAVENs: Motion analysis and visualization of elastic networks and structural ensembles. *BMC Bioinf. 12*, 264.

DOI: 10.1021/acs.biochem.5b00042
Biochemistry 2015, 54, 3543−3554